

# Efficient energy transfer in light-harvesting systems, III: The influence of the eighth bacteriochlorophyll on the dynamics and efficiency in FMO

Jeremy Moix

*Department of Chemistry, Massachusetts Institute of Technology,*

*77 Massachusetts Avenue, Cambridge, MA 02139*

*Singapore MIT Alliance for Research and Technology,*

*18 Medical Drive, Singapore 117456 and*

*School of Materials Science and Engineering,*

*Nanyang Technological University, Singapore 639798*

Jianlan Wu

*Department of Physics, Zhejiang University,*

*38 ZheDa Road, Hangzhou, China, 310027 and*

*Singapore MIT Alliance for Research and Technology,*

*18 Medical Drive, Singapore 117456*

Pengfei Huo and David Coker

*Department of Chemistry, Boston University,*

*590 Commonwealth Avenue, Boston, Massachusetts 02215, USA and*

*Department of Physics, University College Dublin, Dublin 4, Ireland*

Jianshu Cao\*

*Department of Chemistry, Massachusetts Institute of Technology,*

*77 Massachusetts Avenue, Cambridge, MA 02139 and*

*Singapore MIT Alliance for Research and Technology,*

*18 Medical Drive, Singapore 117456*

(Dated: September 16, 2011)

## Abstract

The most recent crystal structure of the Fenna-Matthews-Olson (FMO) protein complex indicates that each subunit contains an additional eighth chromophore. It has been proposed that this extra site functions as a link between the chlorosome antenna complex and the remaining seven chromophores in FMO [Schmidt am Busch et al, *J. Phys. Chem. Lett.*, **2**, 93 (2011)]. Here, we investigate the implications of this scenario through numerical calculations with the generalized Bloch-Redfield (GBR) equation and the non-interacting blip approximation (NIBA). Three key insights into the population dynamics and energy transfer efficiency in FMO are provided. First, it is shown that the oscillations that are often observed in the population relaxation of the dimer composed of sites one and two may be completely suppressed in the eight site model. The presence of the coherent oscillations is shown to depend upon the particular initial preparation of the dimer state. Secondly it is demonstrated that while the presence of the eighth chromophore does not cause a dramatic change in the energy transfer efficiency, it does however lead to a dominant energy transfer pathway which can be characterized by an effective three site system arranged in an equally-spaced downhill configuration. Such a configuration leads to an optimal value of the site energy of the eighth chromophore which is shown to be near to its suggested value. Finally we confirm that the energy transfer process in the eight site FMO complex remains efficient and robust. The optimal values of the bath parameters are computed and shown to be closer to the experimentally fitted values than those calculated previously for the seven site system.

## I. INTRODUCTION

The Fenna-Matthews-Olson (FMO) protein is one of the simplest and most well-studied light harvesting systems. The protein complex exists as a trimer of three identical subunits whose function is to link the chlorosome antenna complex, where light-harvesting takes place, with the reaction center, where charge separation occurs. FMO is also one of the earliest light harvesting systems for which a high resolution crystal structure has been obtained.<sup>1</sup> This early crystal structure indicated that each of the three FMO subunits contains seven Bacteriochlorophyll (Bchl) chromophores which serve as the primary energy transfer pathway between the chlorosome and the reaction center.<sup>2-5</sup> Recently, however, a more careful crystallographic analysis of FMO has been performed which demonstrates that the individual subunits contain eight Bchls, not seven.<sup>6,7</sup> The eighth Bchl resides on the surface of the protein complex and it has been suggested that this additional chromophore is often lost during sample preparation.

From an energy transfer perspective, the presence of an additional chromophore may challenge current understanding of how exciton transfer occurs in FMO. For example, in many previous studies on the seven Bchl complex, it is thought that two nearly independent energy transfer pathways exist.<sup>8-12</sup> Sites one and six are approximately equidistant from the antenna complex and both are assumed to be possible locations for accepting the excitation from the chlorosome. From there, the energy is subsequently funneled either from site one to two (pathway 1) or from site six to sites seven, five, and four (pathway 2). The terminal point through either route is site three where the exciton is then transferred to the reaction center (see Fig. 2(a)). The couplings within each of the pathways are much larger than the couplings between the two which implies that the two routes are nearly independent.<sup>9,12,13</sup> In the second paper of this series, the two pathways and the respective probability of traversing each have been quantified using a flux analysis.<sup>12</sup>

However, this two pathway picture is not entirely consistent with the recent experimental data. The new crystal structure indicates that the eighth chromophore resides roughly midway between the baseplate and the Bchl at site one.<sup>6,7,14</sup> Additionally, Renger and coworkers argued in Ref. 14 that the eighth Bchl provides the most efficient path for exciton injection into FMO as a result of its position and orientation with respect to the chlorosome. If this is correct and site eight serves as the primary acceptor of excitation energy from the chloro-

some, then a preferential energy transfer route emerges through pathway 1. Due to the weak inter-pathway couplings, the secondary channel involving the remaining four chromophores in pathway 2 is largely bypassed in this scheme. This observation may have a significant impact on the efficiency and robustness of the energy transfer process. The main objective of this work is to address this issue by exploring how the dynamics and the energy transfer efficiency in FMO are affected by the presence of the eighth site and a realistic environment.

The first major conclusion of the present study is related to the population dynamics in FMO. In many of the the previous studies of the seven site model of FMO, the population relaxation dynamics are modeled with site one or site six initially populated.<sup>8–11</sup> Under either of these initial conditions, pronounced oscillations in the short-time dynamics are observed. However when site eight is initially excited,<sup>14</sup> then the oscillations in the populations are completely suppressed. This lack of oscillations has been independently observed in the dynamics recently reported in Refs. 14–16. Here, we provide a simple explanation for this behavior. The eighth Bchl maintains a large energy gap with the other seven sites in FMO in order to facilitate efficient directed energy transport. However, it is also rather weakly coupled to the remaining Bchl. This leads to a slow incoherent decay of the initial population at site eight, and hence a broad distribution of initial conditions at the dimer. The consequence of this result is that the population oscillations generally observed between sites one and two are completely suppressed which illustrates the importance of the initial conditions on the dynamics of the dimer.

The second key result of this work demonstrates that if the eighth Bchl is the primary acceptor of excitation energy from the chlorosome as recently proposed then a primary energy transfer pathway in FMO does indeed emerge.<sup>14</sup> Note that this situation is substantially different from the previous interpretations of the energy flow in the seven site models where two independent pathways are generally assumed to exist. The extent of this effect and its impact on the energy transfer efficiency is quantified by introducing reduced models of FMO that consist of only a subset of the sites in the full system. It is demonstrated that sites eight, one, two and three which constitute pathway 1 provide the largest contribution to the dynamics of the full system. The remaining four sites of pathway 2 are seen to play a relatively small role. Despite the fact that only a single pathway dominates the energy transfer process, we also show that the presence of the extra Bchl does not significantly impact the efficiency or robustness of FMO. The eight site model leads to only a slight

increase in the transfer time as compared with the seven site system, and thus maintains the same high efficiency as observed in previous studies of FMO.

Based upon energetic arguments, it has been suggested that the presence of the eighth Bchl leads to optimal energy transfer in FMO.<sup>14</sup> That is, its location near the chlorosome allows for a large coupling to the antenna complex as well as substantial overlap of the absorption spectrum of the eighth Bchl with the fluorescence spectrum of the chlorosome. These factors result in efficient transfer of the excitation energy into FMO while simultaneously allowing the eighth chromophore to maintain a large energy gap with the remaining Bchls and hence a favorable energy transport landscape. These features implicitly suggest that there should be an optimal value of the site energy of the eighth Bchl. Here it is demonstrated that this observation is correct. However, in this case, the behavior is independent of the presence of the chlorosome, and can be understood by considering a further reduction pathway 1 to only three sites. The result of this procedure is a downhill configuration of three equally spaced sites (see Fig. 2(c)) which is known to allow for highly efficient energy transfer.<sup>17</sup>

Recently, several studies have shown that the environment does not have an entirely destructive role in the energy transport properties of excitonic systems.<sup>11,12,18–20</sup> Instead, the environment can serve to enhance both the efficiency and robustness of the energy transfer process. Optimal values have been shown to exist for the temperature as well as other bath parameters which maximize the energy transfer efficiency in several light harvesting systems. Moreover, the experimentally fitted model parameters for FMO are near optimal in many cases. An extensive search for the optimal environmental parameters has been recently presented in Refs. 11 and 21. In addition to the above findings, we also explore the effect of the eighth Bchl on the environmentally assisted energy transport properties in FMO. It is found that the optimal values of the bath parameters are similar to those found in the seven site model, but are closer to the experimental values in general. As has been observed before, the energy transfer efficiency is relatively stable over a broad range of parameters illustrating the robustness of the network.<sup>11</sup>

In the next section, we present the average trapping time formalism which is used in the remainder of the discussion as a measure of the energy transfer efficiency.<sup>11,22</sup> This is followed by a brief outline of the generalized Bloch-Redfield (GBR) approach and the model Hamiltonian for the eight site FMO complex used in the numerical calculations. The results

for the population dynamics and the development of the reduced models for FMO are then presented in Sec. III. This is followed by calculations of the trapping time as a function of the site energies and bath parameters. There it is demonstrated that optimal values exist for many of these parameters, and additionally that the experimentally fitted values for FMO are near-optimal.

## II. METHODS

### A. Average Trapping time

The formalism for calculating the averaging trapping time in light harvesting systems has been presented in detail previously in Refs. 17 and 11. Here we provide only the salient results. The total system is characterized by a discrete  $N$ -site system Hamiltonian,  $H_s$  and its interaction with the environment,  $H_{sb}$ . Each site of the system is coupled to an independent bath of harmonic oscillators with the respective Hamiltonians,  $H_b = \frac{1}{2} \sum_j (p_j^2 + \omega_j^2 x_j^2)$ . The total Hamiltonian is then given by,

$$H = \sum_n^N \epsilon_n |n\rangle \langle n| + \sum_{n \neq m}^N V_{nm} |n\rangle \langle m| + \sum_n^N |n\rangle \langle n| \left[ H_b^{(n)} + \sum_j c_j^{(n)} x_j^{(n)} \right], \quad (1)$$

where  $c_j^{(n)}$  denotes the coupling coefficient of site  $n$  to the  $j$ -th mode of its associated bath. The values of the site energies,  $\epsilon_n$ , and couplings constants,  $V_{nm}$ , are specified below in Sec. II D.

The time evolution of the reduced density matrix of this system can be conveniently described in the Liouville representation as,

$$\begin{aligned} \frac{\partial \rho(t)}{\partial t} &= -L_{\text{tot}} \rho(t) \\ &= - (L_s + L_{\text{trap}} + L_{\text{decay}} + L_{\text{sb}}) \rho(t), \end{aligned} \quad (2)$$

where  $L_s \rho = i/\hbar [H_s, \rho]$  describes the coherent evolution under the bare system Hamiltonian  $H_s$ . In light harvesting systems, the energy flows irreversibly to the reaction center which is modeled here through the trapping operator  $[L_{\text{trap}}]_{nm,nm} = (k_{t_m} + k_{t_n})/2$ , where  $k_{t_n}$  denotes the trapping rate at site  $n$ . The energy transfer in FMO exhibits almost unit quantum yield. As a result, the decay rate of the excitation at any site to the ground state,  $k_d$ , is expected

to be much smaller than the trapping rate,  $k_t \gg k_d$ . This allows for the simplification  $L_{\text{decay}} = 0$ .

## B. Generalized Bloch-Redfield Equation

It remains to account for the Liouville operator describing the system-bath coupling  $L_{\text{sb}}$  in Eq. 2. For a harmonic bath linearly coupled to the system, the time correlation function of the bath coupling operators is given by the standard relation<sup>23,24</sup>

$$C(t) = \frac{1}{\pi} \int_0^\infty d\omega J(\omega) \left( \coth\left(\frac{\hbar\beta\omega}{2}\right) \cos(\omega t) - i \sin(\omega t) \right), \quad (3)$$

where  $\beta = 1/k_B T$  and  $J(\omega) = \frac{\pi}{2} \sum_j \frac{c_j^2}{\omega_j} \delta(\omega - \omega_j)$  is the spectral density of the bath. For simplicity, we assume the spectral density is the same for each of the independent baths and given by the Drude form

$$J(\omega) = 2\lambda\omega_c \frac{\omega}{\omega^2 + \omega_c^2}, \quad (4)$$

where  $\lambda$  is the bath reorganization energy and  $\omega_c$  is the Debye cutoff frequency. For this special choice, the correlation function may be expanded in terms of the Matsubara frequencies,  $\nu_j = \frac{2\pi j}{\hbar\beta}$ , as<sup>11,23,24</sup>

$$\begin{aligned} C(t) &= \left( \frac{2\lambda}{\hbar\beta} + \frac{4\lambda\omega_c}{\hbar\beta} \sum_{j=1}^{\infty} \frac{\omega_c}{\omega_c^2 - \nu_j^2} - i\lambda\omega_c \right) e^{-\omega_c t} - \frac{4\lambda\omega_c}{\hbar\beta} \sum_{j=1}^{\infty} \frac{\nu_j}{\omega_c^2 - \nu_j^2} e^{-\nu_j t} \\ &= \sum_{j=0}^{\infty} \alpha_j e^{-\nu_j t}, \end{aligned} \quad (5)$$

which defines the complex expansion coefficients  $\alpha_j$  with the condition  $\nu_0 = \omega_c$ .

The dynamics in FMO have been computed using a variety of methods ranging in both accuracy and cost.<sup>9,10,13,15,21,25</sup> Here, we choose the approximate generalized Bloch-Redfield (GBR) method which follows from a second order cumulant expansion in the system-bath interaction. It provides an accurate, but computationally friendly approach for the propagation of the density matrix over much of the physically relevant parameter space.<sup>11,22</sup> Due to the decomposition of the bath autocorrelation function in Eq. 5, the system-bath interaction may be accounted for through the introduction of auxiliary fields. The GBR equation of motion for the reduced density matrix is then given by

$$\frac{\partial \rho(t)}{\partial t} = - (L_{\text{sys}} + L_{\text{trap}}) \rho(t) - i \sum_n \sum_{j=0}^{\infty} [A_n, g_{n,j}(t)]. \quad (6)$$

The coupling of each Bchl to an independent bath leads to the additional sum over the  $N$  sites where the system operator  $A_n = |n\rangle \langle n|$  and  $g_{n,j}$  denotes the  $j$ th-auxiliary field coupled to site  $n$ . The auxiliary variables are subject to the initial conditions  $g_{n,j}(0) = 0$  and obey the equations of motion,

$$\frac{\partial g_{n,j}(t)}{\partial t} = - (L_{\text{sys}} + L_{\text{trap}} + \nu_j) g_{n,j}(t) - i \text{Re}(\alpha_j) [A_n, \rho(t)] + \text{Im}(\alpha_j) [A_n, \rho(t)]_+ , \quad (7)$$

where the plus subscript denotes anti-commutation.

### C. Trapping Time

The mean residence time at site  $n$  is by definition

$$\langle \tau_n \rangle = \int_0^\infty dt \rho_{nn}(t) , \quad (8)$$

where  $\rho_{nn}$  denotes the population at site  $n$ . The average trapping time is then given simply as the sum of the residence times at each of the  $N$  sites,  $\langle t \rangle = \sum_{n=1}^N \langle \tau_n \rangle$ . Invoking the steady state solution of Eq. 2,  $L_{\text{tot}} \langle t \rangle = \rho(0)$ , then the average trapping time is given by the compact expression,

$$\langle t \rangle = \text{Tr} (L_{\text{tot}}^{-1} \rho(0)) , \quad (9)$$

where the trace is taken over the site populations of the reduced density matrix.

### D. Eight Site FMO model

The Hamiltonian for FMO is constructed from the crystal structure recently deposited in the protein data bank (pdb code: 3eoj).<sup>7</sup> The site energies are taken from those computed in Ref. 14 and the coupling element between sites  $n$  and  $m$  is calculated from the dipole-dipole approximation,

$$V_{nm} = C \left( \frac{\mathbf{d}_n \cdot \mathbf{d}_m}{|\mathbf{r}_{nm}|^3} - 3 \frac{(\mathbf{d}_n \cdot \mathbf{r}_{nm})(\mathbf{d}_m \cdot \mathbf{r}_{nm})}{|\mathbf{r}_{nm}|^5} \right) . \quad (10)$$

Additional details and the explicit system Hamiltonian are given in the Appendix. Aside from the eighth site, the most significant difference between the present model Hamiltonian and the model previously derived by Cho et al.<sup>26</sup> is in the energy difference between sites one and two. In the current case, the energy transfer through pathway 1 is entirely energetically favorable whereas a barrier is present between site one and two in the model of Ref. 26.

Unless otherwise stated, the bath is characterized by the experimentally fitted values for the reorganization energy of  $35 \text{ cm}^{-1}$  and Debye frequency  $\omega_c^{-1} = 50 \text{ fs}$  ( $105 \text{ cm}^{-1}$ ).<sup>8,26</sup> Additionally the temperature is 300 K and the trap is located at site three with a trapping rate of  $k_t = 1 \text{ ps}^{-1}$ .

### III. NUMERICAL RESULTS

#### A. Population Dynamics and suppression of the oscillations

The time evolution of the populations in the eight site model of FMO calculated from Eq. 2 using the GBR is shown in Fig. 1(a) and (b) for the initial population located at site one and site eight, respectively. The bath parameters are taken at their fitted values specified above and the trap at site three is not included. The most striking difference seen between Fig. 1(a) and (b) is the absence of the oscillations in the populations of the dimer when site eight is initially excited. Other recent studies of the eight site model of FMO have also observed a similar lack of oscillations.<sup>14–16</sup> The origin of this effect may be traced to the initial conditions at the dimer. The energy difference between site eight and the remaining sites is much larger than any of its respective couplings. This leads to the rather slow incoherent exponential relaxation of the population of site eight seen in Fig. 1(b). The resulting initial conditions at sites one and two are then given by a corresponding incoherent distribution. It is this dephasing that suppresses the oscillations generally observed in the dynamics of the dimer.

By applying the non-interacting blip approximation (NIBA) to the spin-boson model, Pachon and Brumer established that a necessary condition for the presence of the oscillations in the dimer is an effective low temperature.<sup>25</sup> The results of Fig. 1 demonstrate that the initial conditions impose an additional constraint on the observation of population oscillations. Note that there are a variety of other initial preparations –such as starting from an eigenstate of the total system or exciting the system with incoherent light<sup>27</sup>– which will also suppress the oscillations in the dimer.

In order to analyze the influence of the initial conditions in more detail, the dynamics of the dimer calculated using the NIBA are presented in Fig. 1(c) and (d). The population dynamics described in Ref. 25 may be formulated as an equivalent generalized master

equation<sup>28–30</sup>

$$\frac{\partial P_n(t)}{\partial t} = \int_0^t dt' \sum_{m=1}^N K_{nm}(t-t') P_m(t') , \quad (11)$$

where  $P_n(t)$  denotes the population of site  $n$  at time  $t$ . The elements of the time-dependent transition matrix are constructed in the standard fashion<sup>31</sup>

$$K_{nm}(t) = (1 - \delta_{nm}) W_{mn}(t) - \delta_{nm} \sum_k W_{nk}(t) \quad (12)$$

where  $\delta_{nm}$  is the Kronecker delta function and the individual rate kernels are given by the NIBA

$$W_{nm}(t) = 2 V_{nm}^2 e^{i(\epsilon_n - \epsilon_m - 2\lambda)t - 2C(t)} . \quad (13)$$

As defined previously, the coupling between site  $n$  and  $m$  is denoted by  $V_{nm}$ ,  $\epsilon_n$  is the energy of site  $n$ ,  $\lambda$  is the reorganization energy, and  $C(t)$  is the bath correlation function given in Eq. 5. The results shown in Fig. 1(c) are calculated from Eq. 11 with the initial population located at site one and are seen to capture the key features of the full GBR dynamics shown in Fig. 1(a). The decay is accounted for by setting the transfer elements  $K_{n1}$  and  $K_{n2}$  to zero for all sites  $n > 2$  which allows for population transfer from the dimer to the remaining Bchls, but prevents any back-transfer. Effectively this results in the addition of traps at sites one and two and thus leads to the population decay of the dimer. Without this decay, the two-site dynamics reproduce those of Ref. 25.

As has been alluded to previously, the lack of oscillations in the dimer when the initial population is located at site eight may be explained by creating a distribution of initial conditions at site one. All of the population is initially located at site one in Fig. 1(a), whereas in Fig. 1(b), the corresponding initial conditions are given by the population that steadily flows from site eight. This slow incoherent decay of the population at site eight may be adequately fit to the single exponential  $P_8(t) = \exp(-\gamma t)$  where  $\gamma = 3 \text{ ps}^{-1}$ . Assuming that site eight decays only into site one, then the population of the latter is given by  $1 - P_8(t)$ , and the corresponding transition rate is  $W_{81}(t) = \gamma \exp(-\gamma t)$ . The influence of site eight on the oscillatory behavior of the dimer can then be captured by convoluting the dynamics given in Fig. 1(c) (denoted by  $P_n(t)$ ) with this initial condition,<sup>32</sup>

$$\bar{P}_n(t) = \int_0^t dt' P_n(t-t') W_{81}(t') . \quad (14)$$

The result of this procedure is shown in Fig. 1(d). As is evident, the oscillatory behavior has completely disappeared. For large  $\gamma$ , the transition rate becomes a delta function and the

dynamics of Fig. 1(c) are recovered. However, oscillations in the populations of both states can be observed only if the decay rate out of site eight is increased fivefold. The presence or absence of the trap simply effects the long time decay of the dimer populations and is irrelevant for the short time oscillatory behavior. These results demonstrate the importance of the initial preparation of the populations on the oscillations in the dynamics.

It should be noted that while the NIBA calculations lead to qualitatively similar population dynamics as those given by the GBR, neither of the two approaches are exact. In FMO and other light harvesting systems, many of the model parameters are of the same order of magnitude. For instance, the couplings,  $V_{nm}$ , and energy differences,  $\epsilon_n - \epsilon_m$ , as well as the reorganization energy,  $\lambda$ , and thermal energy,  $\beta^{-1}$ , are all of comparable magnitude. As a result, methods based upon second-order perturbation theory are, in general, insufficient to quantitatively describe the dynamics. A systematic procedure for computing higher-order contributions to the NIBA rates has been derived and recently implemented.<sup>12,30</sup> This leads to non-negligible corrections to the dynamics in the spin-boson model, FMO and LH2.<sup>33</sup> Thus while the results in Fig. 1 and those of Ref. 25 capture the qualitative features that are necessary to analyze the energy transfer behavior, there will be quantitative corrections from higher order terms.

## B. Pathway analysis and the ladder configuration

Regardless of the presence or absence of oscillations, it is readily seen from Fig. 1(a) and (b) that the population primarily flows through pathway 1. Among the sites in pathway 2, only site four ever accumulates more than ten percent of the population. Particularly for times less than 500 fs, the sites from pathway 2 are scarcely populated. Similar behavior of the population dynamics has been seen in many other simulations of the seven site model for FMO.<sup>9,10,13–16</sup> These observations lead to the first reduced model for FMO which consists of only the four sites in pathway one shown in Fig. 2(b). As demonstrated below, this model is able to accurately capture the key features of the energy transfer process. One may proceed further by noting that sites one and two are coupled more strongly than the energy difference between the two. Additionally, sites eight and three are widely separated from either site in the dimer. The couplings between the distant sites and dimer are also rather weak (see values in the model Hamiltonian in Eq. 15 and Fig. 2(b)). As

a result, there can be rapid coherent energy transfer between sites one and two, whereas the transfer to sites eight or three will be comparatively slow. Therefore, when the initial population is located at site eight we may simply assume that these two sites of the dimer behave as one effective site with an energy that is the average of the two ( $270\text{ cm}^{-1}$ ). A similar “mean state” idea for developing this type of reduced model has been suggested in Ref. 34 which explores the behavior of a dimer embedded in the PC645 photosynthetic network. Furthermore, the coupling between site eight and the terminal site, three, is negligibly small. This leads to a three site model for FMO where the couplings are determined by the nearest-neighbor values as shown in Fig. 2(c).

### C. Site Energy of Bchl 8

Fig. 3 displays the average trapping time calculated as a function of the site energy of Bchl eight. It contains two additional key findings of this work. The first is that the trapping time behavior, and hence the efficiency, seen in the eight site model of FMO is largely governed by the sites in pathway 1. The second feature is that an optimal value exists for the site energy of Bchl 8, and moreover, the optimum is near the fitted value determined in Ref. 14. The source of the latter is the highly efficient ladder configuration shown in Fig. 2(c).

The main portion of Fig. 3 displays the average trapping time calculated with the full Hamiltonian given in Eq. 15 along with the corresponding results for the four site model of FMO (see Fig. 2(a) and (b)). The bath parameters are taken at their experimentally fitted values with the temperature of 300 K. The inset of Fig. 3 contains the results from the three sites model shown in Fig. 2(c). For this case, the exact trapping time calculated from the hierarchical equation of motion method is also presented, as well as the results of a Förster theory calculation. As can be seen, both the GBR and the Förster calculations predict optimal values of the site energy that semi-quantitatively capture the behavior of the exact hierarchical results.

These results demonstrate that the energy transport is dominated by a subset of the sites in FMO and furthermore that the mechanism is correctly described by Förster theory. The four site model correctly describes the qualitative features seen in the full system and it accounts for the majority of the trapping time. Of the remaining sites in Fig. 1, site four was seen to have the largest impact on the population relaxation. Calculations that consist

of pathway 1 plus site four are seen to capture almost all of the behavior seen in the full eight site system.

In Ref. 14, it was noted that the site energy of Bchl eight maximizes the overlap with the chlorosome emission spectrum while simultaneously maintaining a large energy gap with the remaining seven core Bchl. This indicates that there should be an optimal value of the site energy of Bchl eight. In addition to the observation that the trapping time behavior may be captured by a simplified model of FMO, there is another interesting feature seen in Fig. 3. The trapping time displays a minimum as a function of the energy of the eighth site for all of the constructed models. Moreover, for the eight site model, the optimal value of the site energy is rather close to the fitted value of  $505\text{ cm}^{-1}$ .<sup>14</sup> Increasing the energy difference between site eight and site one decreases the back-transfer rate, but also decreases the spectral overlap between the two. The position of the optimal value is no coincidence. The three-site model in Fig. 2(c) readily demonstrates that this particular choice for the site energy leads to a downhill configuration of three sites that are approximately equally-spaced and equally-coupled which is known to be very efficient.<sup>17</sup> The qualitative behavior of the trapping time in the full, complicated eight site system becomes obvious with the aid of the reduced models. Note also that the average trapping time varies little over a large range of values of the energy of site eight indicating the robustness of the energy transfer process. Below it is demonstrated that many of the other fitted parameters are near optimal as well.

#### D. Optimal Bath Parameters

The average trapping time calculated as a function of the reorganization energy is shown in Fig. 4(a) and (b). Fig. 4(a) varies the reorganization of all eight sites simultaneously (in this model all chromophores are assumed to have identical environments) whereas (b) varies only that of site eight while keeping all of the others at the fitted value of  $35\text{ cm}^{-1}$ . In order to demonstrate that the presence of the additional chromophore does not lead to a dramatic increase in the trapping time, two different initial conditions are taken with either site one or site eight initially excited. As expected, a slightly larger trapping time is observed with the initial population at site eight due to the larger distance to the trap. However, the difference between the two scenarios is not substantial. Additionally, the qualitative behavior of the two initial conditions is quite similar and both lead to an optimal value of

the reorganization energy that is close to the experimentally fitted value of  $35\text{ cm}^{-1}$ . It has been proposed from recent numerical simulations that the reorganization energy in FMO should be approximately twice as large as the experimentally fitted value used here.<sup>35</sup> The optimal values of  $\lambda$  in Fig. 4(a) ( $55\text{ cm}^{-1}$ ) and (b) ( $40\text{ cm}^{-1}$ ) are consistent with a somewhat larger value of the reorganization energy. The mean trapping time is more sensitive to variations of the reorganization energy than was observed for the site energy in Fig. 3, but there is still a large range of  $\lambda$  where the trapping time is near optimal.

Finally, Fig. 4(c) and (d) display the results for the average trapping time calculated as a function of the Debye frequency and as a function of the temperature. As in Fig. 4(a) two initial conditions are shown with the initial population at either site one or site eight. Again, the average trapping time from site one is always faster than for site eight. Nevertheless, the two initial conditions display qualitatively similar behavior for both the temperature and Debye frequency. Additionally an optimal value of the Debye frequency is observed that is close to the experimentally fitted value of  $105\text{ cm}^{-1}$ . These results for the average trapping time as a function of the bath parameters are similar to those observed previously for the seven site model of FMO.<sup>11</sup> There is one notable difference however. In all cases, the Hamiltonian for the eight site FMO model recently proposed by Renger et al<sup>14</sup> leads to optimal conditions that are closer to the experimentally fitted values than those calculated previously<sup>11</sup> using the Hamiltonian of Ref. 26.

#### IV. CONCLUSIONS

The FMO protein serves as one of the model light harvesting systems, and the qualitative features of the energy transfer process have been understood for some time. However, recent experimental evidence has shown that many of the previously developed theoretical models are not entirely complete. An additional chromophore is present in each subunit of FMO that resides between the chlorosome and site one. In this work we have shown that the presence of the eighth site does not significantly alter the previous conclusions that have been reached with regards to environmentally-assisted exciton transport.<sup>11</sup> Optimal values exist for many of the bath parameters and, moreover, the optimal conditions are generally closer to their respective experimentally fitted values than in the seven site FMO models. Additionally, the dependence of the average trapping time with respect to variations of the

bath parameters is rather weak illustrating the overall robustness of the energy transfer process.

However, the presence of the eight Bchl may necessitate a reassessment of our understanding of the energy transport process in FMO. Given that site eight is the primary entry point for the exciton into FMO, then Fig. 1 clearly exhibits a complete suppression of the population oscillations that are generally observed in the seven site models of FMO. That is, the coherent population oscillations observed in previous studies depend upon the special choice of initial conditions. Here we have shown that the origin of the suppression is the slow decay of the initial population at site eight which leads to an incoherent distribution of initial conditions at the dimer. In the physical setting there will be an additional source of dephasing due to the extra step from the chlorosome to FMO. This will broaden the distribution of initial conditions even more and further suppress the oscillations in the dimer.

An additional feature of the eight site model that is markedly different from the previous seven site configuration is observed in the population dynamics shown in Fig. 1 and the average trapping times displayed in Fig. 3. These results demonstrate that the energy flow in the eight site model is dominated by a subset of the chromophores, whereas it has been previously assumed that two independent pathways involving all of the Bchl are available for the energy transfer process. The qualitative features of the transport in the eight site model are largely determined by the dynamics of pathway 1. Sites four, five, six and seven provide a rather small contribution to the overall efficiency in this case. The agreement between the results for the full eight site system and the reduced four- and three-site models shown in Fig. 2 provide further support to this claim. Nevertheless, the eight site model and the seven site model display similar energy transport efficiencies. The origin of this behavior in the former is evident from Fig. 2(c) which shows that the eighth Bchl forms an optimal downhill ladder configuration with the dimer and site three. This result demonstrate the usefulness of the reduced models in providing an intuitive explanation of many of the key features present in the numerical results.

## V. ACKNOWLEDGMENT

This work was supported by grants from the National Science Foundation, DARPA, the Center for Excitonics at MIT, the MIT energy initiative (MITEI), and the Singapore-MIT alliance for research and technology (SMART)

## VI. APPENDIX

Following the prescriptions used previously for constructing the dipole-dipole interactions,<sup>14,36,37</sup> the unit vectors,  $\mathbf{d}_n$ , in Eq. 10 point along the axis connecting the  $N_b$  and  $N_d$  atoms of the  $n$ -th Bchl and  $\mathbf{r}_{nm}$  is the vector connecting the Mg atoms of Bchl  $n$  and  $m$ . Setting the constant  $C = 155000 \text{ cm}^{-1}\text{\AA}^3$  leads to an effective dipole strength of 30 D<sup>2</sup>. With these specifications, the system Hamiltonian (in cm<sup>-1</sup>) for the eight site model is

$$H_{\text{FMO}} = \begin{pmatrix} 310.0 & -97.9 & 5.5 & -5.8 & 6.7 & -12.1 & -10.3 & 37.5 \\ -97.9 & 230.0 & 30.1 & 7.3 & 2.0 & 11.5 & 4.8 & 7.9 \\ 5.5 & 30.1 & 0.0 & -58.8 & -1.5 & -9.6 & 4.7 & 1.5 \\ -5.8 & 7.3 & -58.8 & 180.0 & -64.9 & -17.4 & -64.4 & -1.7 \\ 6.7 & 2.0 & -1.5 & -64.9 & 405.0 & 89.0 & -6.4 & 4.5 \\ -12.1 & 11.5 & -9.6 & -17.4 & 89.0 & 320.0 & 31.7 & -9.7 \\ -10.3 & 4.8 & 4.7 & -64.4 & -6.4 & 31.7 & 270.0 & -11.4 \\ 37.5 & 7.9 & 1.5 & -1.7 & 4.5 & -9.7 & -11.4 & 505.0 \end{pmatrix}, \quad (15)$$

where the zero of energy is 12195 cm<sup>-1</sup>. Note that there is an error in the sign of the coupling between sites one and two in the table provided in Ref. 14. Aside from this, these values reproduce all of the couplings listed therein to within 3 cm<sup>-1</sup>.

---

\* Electronic address: jianshu@mit.edu

<sup>1</sup> R. E. Fenna and B. W. Matthews, *Nature* **258**, 573 (1975).

<sup>2</sup> T. Brixner, J. Stenger, H. M. Vaswani, M. Cho, R. E. Blankenship, and G. R. Fleming, *Nature* **434**, 625 (2005).

<sup>3</sup> G. S. Engel, T. R. Calhoun, E. L. Read, T. Ahn, T. Mancal, Y. Cheng, R. E. Blankenship, and G. R. Fleming, *Nature* **446**, 782 (2007).

<sup>4</sup> G. Panitchayangkoon, D. Hayes, K. A. Fransted, J. R. Caram, E. Harel, J. Wen, R. E. Blankenship, and G. S. Engel, Proc. Natl. Acad. Sci. USA **107**, 12766 (2010).

<sup>5</sup> E. Collini, C. Y. Wong, K. E. Wilk, P. M. G. Curmi, P. Brumer, and G. D. Scholes, Nature **463**, 644 (2010).

<sup>6</sup> A. Ben-Shem, F. Frolov, and N. Nelson, FEBS Letters **564**, 274 (2004).

<sup>7</sup> D. E. Tronrud, J. Wen, L. Gay, and R. E. Blankenship, Photosynth. Res. **100**, 79 (2009).

<sup>8</sup> A. Ishizaki and G. R. Fleming, J. Chem. Phys. **130**, 234111 (2009).

<sup>9</sup> P. Huo and D. F. Coker, J. Chem. Phys. **133**, 184108 (2010).

<sup>10</sup> G. Tao and W. H. Miller, J. Phys. Chem. Lett. **1**, 891 (2010).

<sup>11</sup> J. Wu, F. Liu, Y. Shen, J. Cao, and R. J. Silbey, New J. Phys. **12**, 105012 (2010).

<sup>12</sup> J. Wu, F. Liu, J. Ma, X. Wang, R. Silbey, and J. Cao (2011), submitted.

<sup>13</sup> A. Ishizaki and G. R. Fleming, Proc. Natl. Acad. Sci. USA **106**, 17255 (2009).

<sup>14</sup> M. Schmidt am Busch, F. Mühl, M. E. Madjet, and T. Renger, J. Phys. Chem. Lett. **2**, 93 (2011).

<sup>15</sup> N. Renaud, M. A. Ratner, and V. Mujica, J. Chem. Phys. **135**, 075102 (2011).

<sup>16</sup> G. Ritschel, J. Roden, W. T. Strunz, A. Aspuru-Guzik, and A. Eisfeld, arXiv:1108.3452 (2011).

<sup>17</sup> J. Cao and R. J. Silbey, J. Phys. Chem. A **113**, 13825 (2009).

<sup>18</sup> M. Mohseni, P. Rebentrost, S. Lloyd, and A. Aspuru-Guzik, J. Chem. Phys. **129**, 174106 (2008).

<sup>19</sup> M. B. Plenio and S. F. Huelga, New J. Phys. **10**, 113019 (2008).

<sup>20</sup> A. W. Chin, A. Datta, F. Caruso, S. F. Huelga, and M. B. Plenio, New J. Phys. **12**, 065002 (2010).

<sup>21</sup> M. Mohseni, A. Shabani, S. Lloyd, and H. Rabitz, arXiv:1104.4812 (2011).

<sup>22</sup> J. Cao, J. Chem. Phys. **107**, 3204 (1997).

<sup>23</sup> U. Weiss, *Quantum Dissipative Systems* (World Scientific, Singapore, 1999), 2nd ed.

<sup>24</sup> S. Mukamel, *Principles of Nonlinear Optical Spectroscopy* (Oxford University Press, USA, 1999).

<sup>25</sup> L. A. Pachon and P. Brumer, arXiv:1107.0322 (2011).

<sup>26</sup> M. Cho, H. M. Vaswani, T. Brixner, J. Stenger, and G. R. Fleming, J. Phys. Chem. B **109**, 10542 (2005).

<sup>27</sup> P. Brumer and M. Shapiro, arXiv:1109.0026 (2011).

<sup>28</sup> R. Silbey and R. A. Harris, J. Chem. Phys. **80**, 2615 (1984).

<sup>29</sup> C. Aslangul, N. Pottier, and D. Saint-James, J. Phys. (Paris) **47**, 5 (1986).

<sup>30</sup> J. Cao, J. Chem. Phys. **112**, 6719 (2000).

<sup>31</sup> R. Zwanzig, *Nonequilibrium statistical mechanics* (Oxford University Press, London, 2001).

<sup>32</sup> R. Kubo, M. Toda, and N. Hashitsume, *Statistical Physics II: Nonequilibrium Statistical Mechanics* (Springer-Verlag, Berlin, 1985), 2nd ed.

<sup>33</sup> J. Wu, R. J. Silbey, and J. Cao (2012), in preparation.

<sup>34</sup> P. Huo and D. F. Coker, J. Phys. Chem. Lett. **2**, 825 (2011).

<sup>35</sup> C. Olbrich, J. Strümpfer, K. Schulten, and U. Kleinekathöfer, J. Phys. Chem. Lett. **2**, 1771 (2011).

<sup>36</sup> X. Hu, T. Ritz, A. Damjanović, and K. Schulten, J. Phys. Chem. B **101**, 3854 (1997).

<sup>37</sup> F. Müh, M. E. Madjet, J. Adolphs, A. Abdurahman, B. Rabenstein, H. Ishikita, E. Knapp, and T. Renger, Proc. Natl. Acad. Sci. USA **104**, 16862 (2007).

## Figures

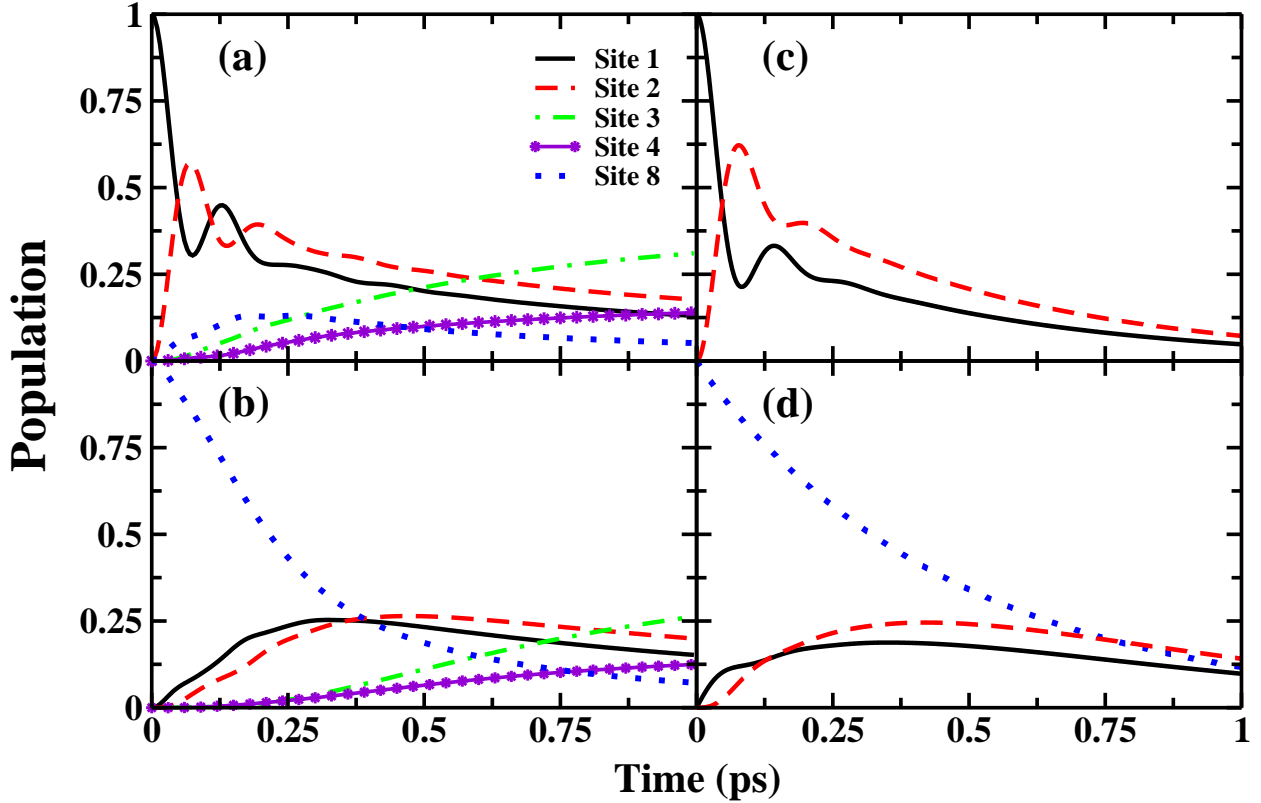


FIG. 1: Site populations of in the eight site model of FMO with Bchl one (a) or eight (b) initially excited calculated with the GBR. The populations of the remaining sites five, six and seven are never larger than 10% and not shown. The site populations of the dimer calculated using the NIBA of Eq. 11 calculated with site one initially excited (c) and from Eq. 14 (d). In all cases, the temperature is 300 K with a reorganization energy of  $35 \text{ cm}^{-1}$  and cutoff frequency of  $\omega_c^{-1} = 50 \text{ fs}$ .

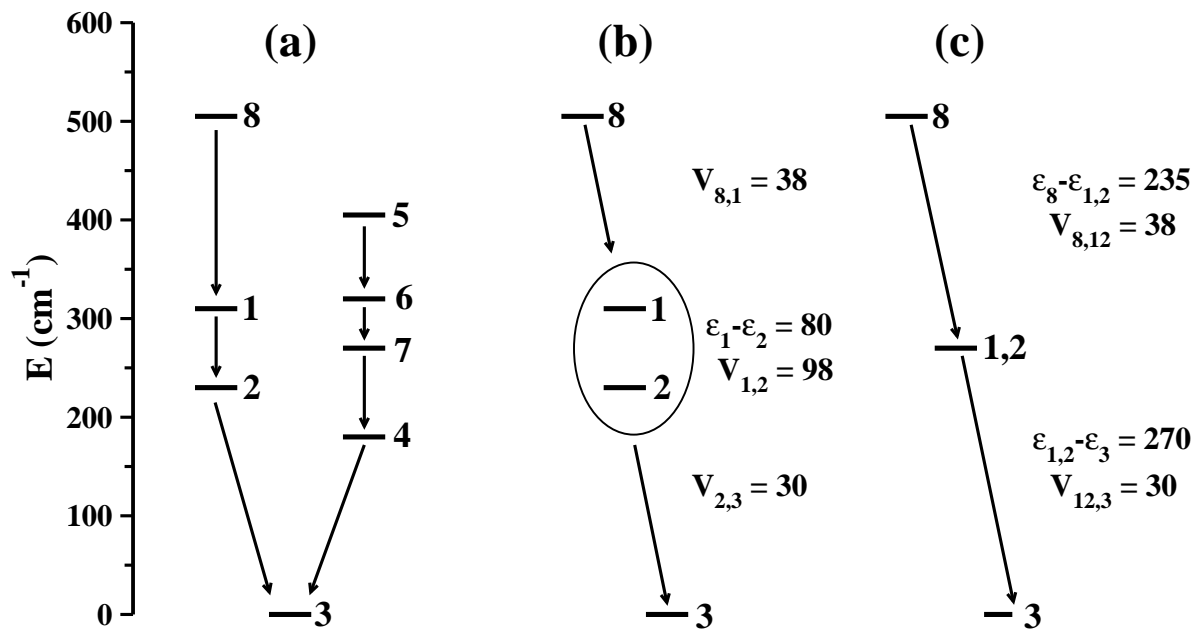


FIG. 2: Energy diagrams for the eight site model (a), the four site model (b), and three site model (c) used in the calculations of Fig. 3.

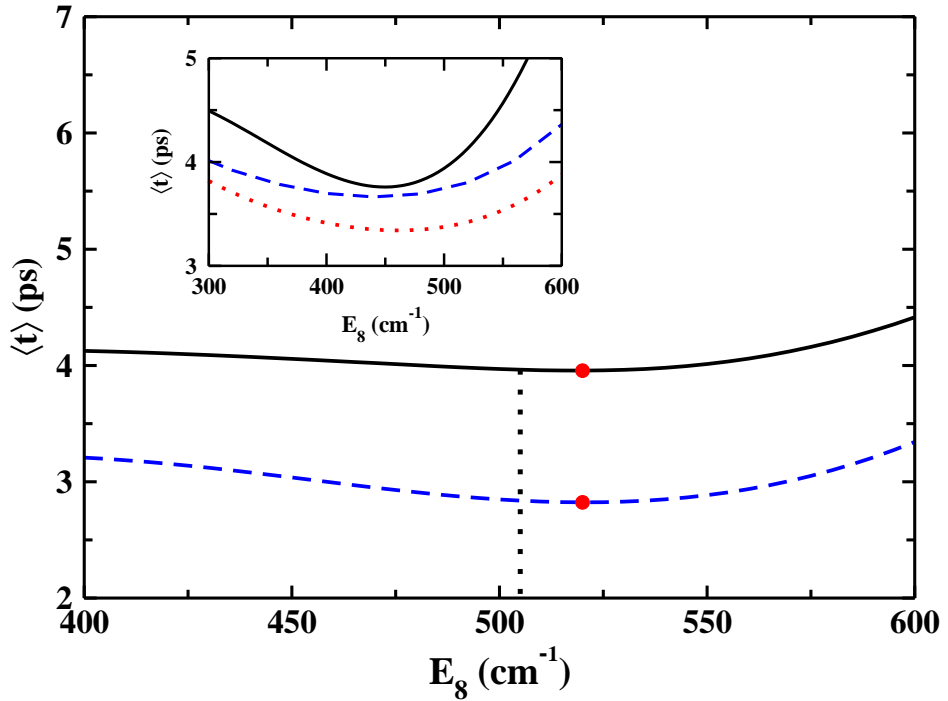


FIG. 3: The trapping time as a function of the site energy of site eight. The solid (black) line and dashed (blue) line in the main figure correspond to the results calculated from the full eight site Hamiltonian of Eq. 15 and with only the four sites of pathway 1, respectively. The red dots correspond to the optimal site energies and the vertical dashed line indicates the fitted value of the site energy of Bchl 8 of  $505\text{ cm}^{-1}$  determined in Ref. 14. The inset contains results for the three site model calculated with the GBR (solid black line), Förster theory (dotted red line), and hierarchical equation of motion (dashed blue line). The remaining parameters are the same as in Fig. 1.

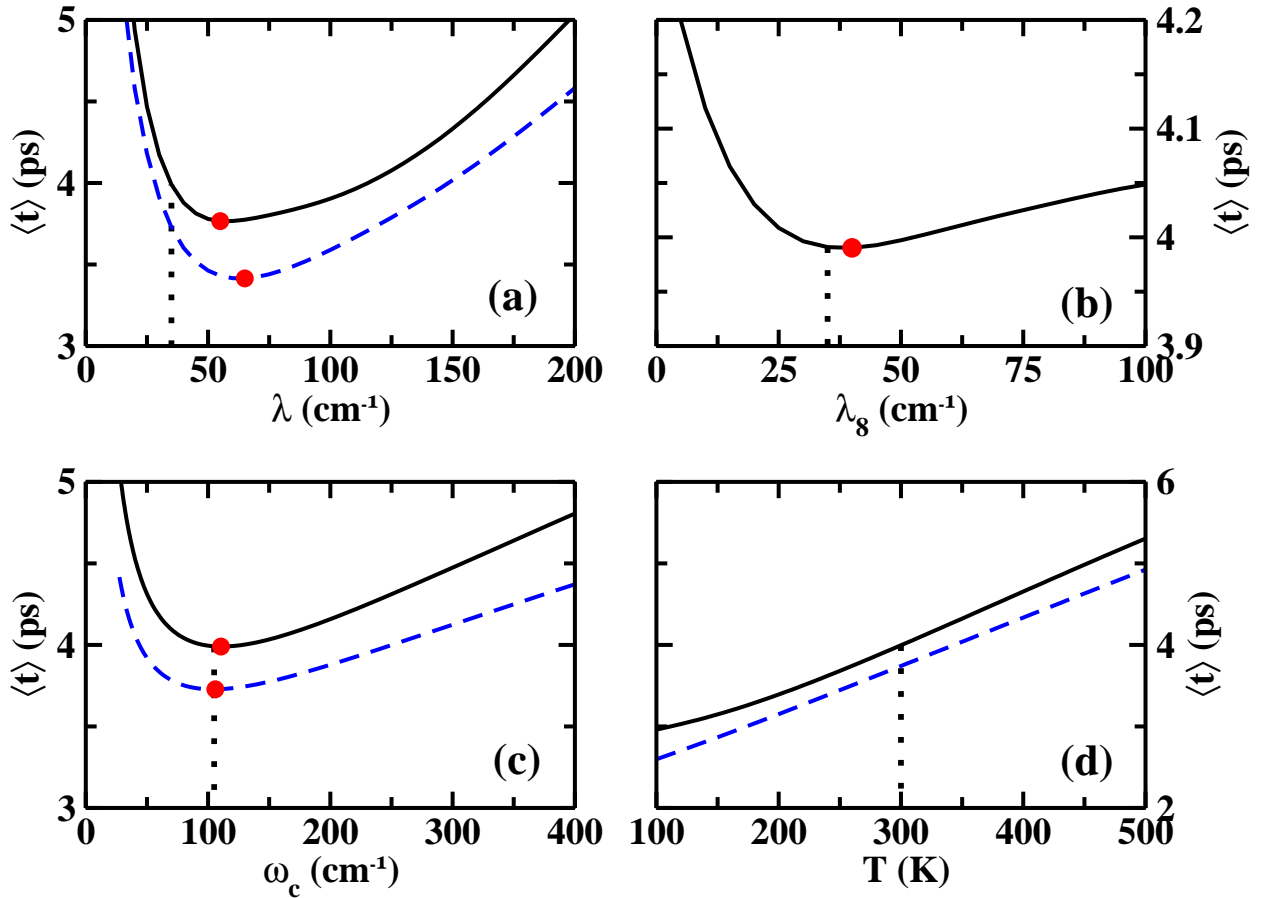


FIG. 4: The trapping time as a function of the reorganization energy of all Bchl (a), and as a function of the reorganization of site eight only (b) while the remaining seven sites are fixed at the experimentally fitted value of  $\lambda = 35 \text{ cm}^{-1}$ . The trapping time as a function of the bath cutoff frequency and temperature are shown in figures (c) and (d) respectively. In all cases the trap rate at site three is 1 ps. The solid (black) and dashed (blue) lines correspond to initial excitation at site eight or site one, respectively. The red dots indicate the optimal trapping times and the dotted vertical lines correspond to the respective experimentally fitted values. The remaining parameters are the same as in Fig. 1.